Correspondence and
requests for materials
should be addressed to
Z.P.L. (luzp@ustb.edu.
cn)

# Enhancing glass-forming ability via frustration of nano-clustering in alloys with a high solvent content

H. X. Li[1], J. E. Gao[1], Y. Wu[1], Z. B. Jiao[1], D. Ma[2], A. D. Stoica[2], X. L. Wang[3], Y. Ren[4], M. K. Miller[2] & Z. P. Lu[1]

[1]State Key Laboratory for Advanced Metals and Materials, University of Science and Technology Beijing, Beijing, 100083, China, [2]Oak Ridge National Laboratory, Oak Ridge, TN 37831, USA, [3]Department of Physics and Materials Science, City University of Hong Kong, Hong Kong, China, [4]Advanced Photon Source, Argonne National Laboratory, Argonne, IL60439, USA.

The glass-forming ability (GFA) of alloys with a high-solvent content such as soft magnetic Fe-based and Al-based alloys is usually limited due to strong formation of the solvent-based solid solution phase. Herein, we report that the GFA of soft magnetic Fe-based alloys (with >70 at.% Fe to ensure large saturation magnetization) could be dramatically improved by doping with only 0.3 at.% Cu which has a positive enthalpy of mixing with Fe. It was found that an appropriate Cu addition could enhance the liquid phase stability and crystallization resistance by destabilizing the $\alpha$-Fe nano-clusters due to the necessity to redistribute the Cu atoms. However, excessive Cu doping would stimulate nucleation of the $\alpha$-Fe nano-clusters due to the repulsive nature between the Fe and Cu atoms, thus deteriorating the GFA. Our findings provide new insights into understanding of glass formation in general.

M etallic glasses with a high solvent content have shown unique physical, magnetic and mechanical properties, which make them attractive for widespread uses as energy and aerospace materials[1–7]. For example, Fe-based metallic glasses such as commercial FINEMET and NANOPERM alloys exhibited a great potential to substitute the silicon steel for saving energy in the electric appliances due to their excellent magnetic softness and low core loss[8–10]. Light-weight Al-based metallic glasses show the good prospect in aerospace application due to the promising mechanical properties[5–7]. To further extend the application range, it imminently demands to improve the glass-forming ability (GFA) simultaneously based on attaining the excellent soft-magnetic properties or outstanding mechanical properties in high-solvent based alloys[11–13]. Nevertheless, the truth is that the high Fe contents in Fe-based amorphous alloys necessary for ensuring large saturation magnetization will inevitably induce structural heterogeneity, usually the $\alpha$-Fe nano-clusters precipitated in the amorphous matrix, which reduces the GFA[14–18]. Thus, obtaining high saturation magnetization in the Fe-based amorphous alloys is always at the expense of the GFA, as shown in the FINEMET and NANOPERM alloys[8–10]. Similarly, high concentration of the solvent in Al-based amorphous alloys normally also induces the strong formation tendency of the $\alpha$-Al clusters and then dramatically deteriorates the GFA[5–7]. Therefore, understanding glass formation and then finding a suitable route to suppress occurrence of the structural heterogeneity in the amorphous matrix will be very crucial for enhancing GFA for such high-solvent based alloys, particularly in the Fe- and Al-based amorphous alloys.

Recently, the element copper, which has a positive mixing enthalpy with Fe (+13 kJ/mol), was often added into the Fe-based amorphous alloys to enhance the soft-magnetic propertie[14–20]. It was argued that copper additions can stimulate nucleation of $\alpha$-Fe and effectively refine the $\alpha$-Fe grain sizes to 20 nm or below. Although these Cu-containing Fe-based metallic glasses have a large saturation magnetization close to that of the conventional Fe-Si alloys, their GFA is reduced and the maximum attainable size is limited to the micrometer level[14–21], which is consistent with the results in the Fe-Co-based alloys[22–24]. In our study, however, we surprisingly found that minor doping of the element Cu is actually very effective in destabilizing the $\alpha$-Fe nano-clusters and promoting the GFA. As a result, soft-magnetic Fe-based bulk amorphous alloys with high GFA and large saturation magnetization simultaneously have been successfully developed. In this report, the relevant experiments are described in detail and the correlation between the nano-clustering and glass formation is discussed. Moreover, the strategy for enhancing the GFA by minor doping the elements, which have positive enthalpy of mixing with the main constituents, is also extended into Al-based amorphous alloys.
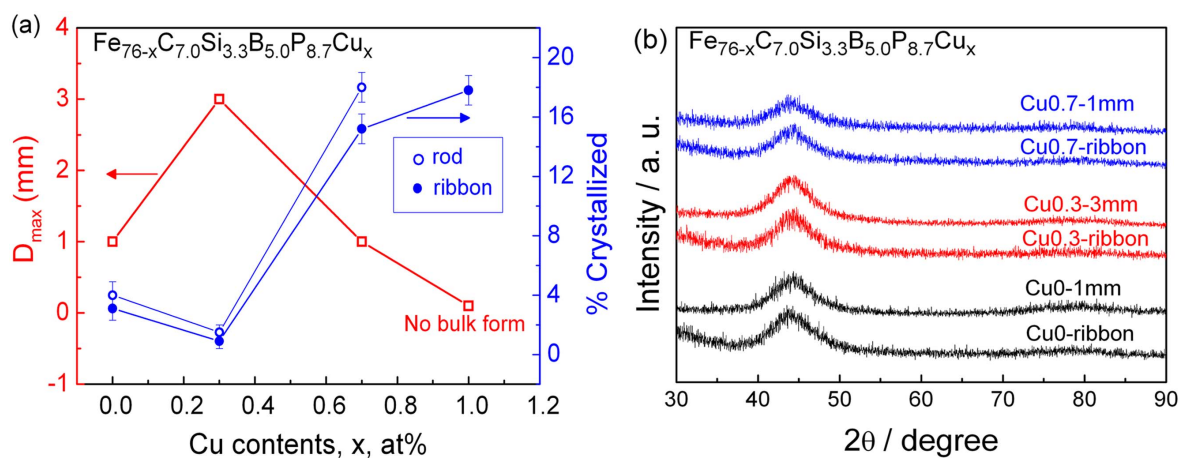
Figure 1 | (a) The maximum attainable diameter ($D_{max}$) for glass formation and the volume fraction of the α-Fe nanocrystals in the ribbons and rods annealed at 729 K for 30 min as a function of the Cu content. (b) XRD patterns of the as-spun ribbon and as-cast rods with the maximum diameter for the $Fe_{76-x}C_{7.0}Si_{3.3}B_{5.0}P_{8.7}Cu_x$ (x = 0, 0.3, 0.7) alloys.

## Results

The maximum attainable diameter ($D_{max}$) for glass formation as a function of the Cu contents and the corresponding XRD patterns for the as-prepared ribbons and rods with different Cu contents are shown in Fig. 1, which clearly demonstrates that GFA of the alloys is very sensitive to the Cu contents. As shown in Figs. 1a and 1b, doping 3000 ppm Cu in the alloy $Fe_{76}C_{7.0}Si_{3.3}B_{5.0}P_{8.7}$ apparently improves the GFA so that the critical diameter is increased from 1 mm to 3 mm. However, excessive Cu doping (e.g., 0.7 %) reduces the GFA and consequently, the critical diameter for glass formation is reduced to only 1 mm. As the Cu doping is increased to 1 %, bulk glass can no longer be formed, which is consistent with the previous results reported by other researchers[9,25].

Minor additions have been proved to be very effective in enhancing the GFA of bulk amorphous alloys in recent years[26–30]. Generally, the added elements have a large negative mixing enthalpy with main constituents in the alloy[29–32]. In the current case, however, copper has a positive enthalpy of mixing with Fe and the optimum doping content is only 0.3 %, suggesting that the mechanism of GFA enhancement is different from the traditional hypotheses. Figure 2a shows DSC scans of the $Fe_{76-x}C_{7.0}Si_{3.3}B_{5.0}P_{8.7}Cu_x$ (x = 0, 0.3, and 0.7 at. %) glassy rods with their maximum diameter at 20 K/min and the insert shows the blowup of the near-$T_g$ fields. The DSC curves of the melt-spun glassy ribbons with the same composition for these alloys are also included in Fig. 2a for comparison. No appreciable difference in the glass transition temperature $T_g$, the onset crystallization temperature $T_x$, and the crystallization process is recognized between the ribbon and rod specimen for all the alloys, indicating the formation of a similar glassy phase. The thermal properties $T_g$, $T_x$ and the corresponding GFA parameters including the supercooled liquid region $\Delta T_x$, the reduced glass transition temperature $T_{rg}$, and GFA parameter γ are also summarized in Table 1. As shown, the parameters $\Delta T_x$, $T_{rg}$, and γ do not reflect well the GFA dependence on the Cu doping level. Neither can the often-cited three empirical rules[33] or conventional theories for glass formation, such as the confusion principle[34] explain the remarkable GFA improvement in the Cu0.3 alloy due to their similar atomic sizes and positive enthalpy of mixing between Fe and Cu atoms[35,36]. Moreover, one can see that almost no obvious glass transition can be observed and the onset crystallization temperature $T_x$ is smaller for the Cu0.7 alloy compared with Cu0 and Cu0.3 alloys (inset of Fig. 2a), indicating its easy precipitation of primary phase. The isothermal crystallization behavior of the Cu0.3 ribbon and rod specimens were investigated at the temperatures of 773, 776, 779 and 782 K, and the corresponding DSC curves are shown in Fig. 3. It can be seen that all the DSC traces

display obvious exothermic peaks after passing a certain incubation time, τ, further confirming that both the as-cast rod and ribbons of the Cu0.3 alloy is amorphous, rather than microcrystalline. Moreover, the incubation time becomes shorter when raising annealing temperature. These facts imply these amorphous specimens crystallized via a nucleation-and-growth process, instead of pure growth of the pre-existing nanosized nuclei[37,38]. Generally, the
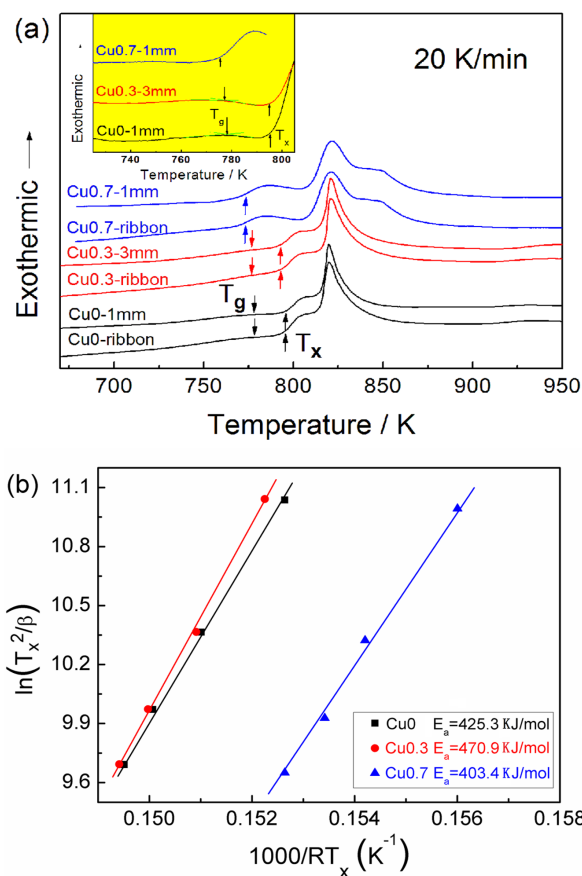


Figure 2 | (a) DSC measurements for the as-spun ribbons and as-cast rods with the inset showing the blowup of the near-$T_g$ field, (b) the corresponding Kissinger plots for estimating the activation energy for crystallization.

**Table 1 | The attainable maximum diameter for glass formation, thermal stability, and activation energy for crystallization obtained by Kissinger analysis for the Cu-free and Cu-doped alloys**

| Alloys | $D_{max}$ (mm) | Thermal stability | | | | | | Activation Energy $E_a$ (kJ/mol) |
|---|---|---|---|---|---|---|---|---|
| | | $T_g$(K) | $T_x$(K) | $T_l$(K) | $\Delta T_x$ (K) | $T_g/T_l$ | $\gamma$ | |
| $Fe_{76.0}C_{7.0}Si_{3.3}B_{5.0}P_{8.7}$ | 1 | 779 | 795 | 1292 | 16 | 0.603 | 0.384 | 425.3 ± 6.8 |
| $Fe_{75.7}C_{7.0}Si_{3.3}B_{5.0}P_{8.7}Cu_{0.3}$ | 3 | 777 | 793 | 1288 | 16 | 0.603 | 0.384 | 470.9 ± 4.2 |
| $Fe_{75.3}C_{7.0}Si_{3.3}B_{5.0}P_{8.7}Cu_{0.7}$ | 1 | — | 774 | 1282 | — | — | — | 403.4 ± 5.6 |
| $Fe_{75.0}C_{7.0}Si_{3.3}B_{5.0}P_{8.7}Cu_{1.0}$ | Ribbon | — | 772 | 1280 | — | — | — | — |

Johnson-Mehl-Avrami (JMA) theory can be used to describe the isothermal crystallization kinetics in metallic glasses[38,39], i.e.,

$$x(t) = 1 - exp\{-[K(t-\tau)]^n\} \qquad (1)$$

where x is the crystallized volume fraction, K a rate constant, t the annealing time period and n the Avrami exponent reflecting the characteristics of nucleation-and-growth during crystallization. The values of K and n can be determined by using the relationship derived from Eq.(1),

$$ln[-ln(1-x) = nlnK + nln(t-\tau)] \qquad (2)$$

It is assumed that the crystallized volume fraction x, up to any time t, is taken as proportional to the fractional area of the exothermic peak. The measured results of x during the isothermal annealing determined by integrating the partial are revealed in Fig. S1. By plotting ln[-ln (1 − x)] versus ln(t − τ) for different temperatures, the JMA plots (x < 40%) can be obtained as shown in Fig. S2. The Avrami exponent n was determined on the basis of the slope and intercept of the straight line are included in Fig. 3. The values of n range from 2.55 to 2.85 for the ribbons and from 2.75 to 2.85 for the rods, and no obvious difference between the n values for the rod and ribbon samples was observed, which implies a diffusion-controlled three-dimensional growth for both ribbons and rods for this particular alloy[40].

To investigate the beneficial roles of the Cu additions, we first analyze the structural heterogeneity of the as-cast specimens via the HRTEM. The corresponding HRTEM images and selected area electron diffraction (SAED) patterns of the as-spun ribbons and the as-cast rods of these alloys are shown in Fig. 4. As expected, formation of 2–3 nm clusters in the amorphous matrix was observed in the Cu0 ribbon, although the SAED pattern still illustrates an obvious amorphous feature with the diffused diffraction ring (Fig. 4a). The lattice fringes as indicated by white bars in Fig. 4a corresponds to the bcc (110) plane distance of a α-Fe crystallite. With addition of 0.3% Cu, fully amorphous phase was obtained with no formation of any

nanosized crystallites (Fig. 4b). Nevertheless, nano-grains with a size of 2–5 nm appeared again in the amorphous matrix of the Cu0.7 ribbon (Fig. 4c).

For the as-cast rods of alloys Cu0 and Cu0.7, similar nano-crystals the amorphous matrix were observed, but the volume fraction of these crystals was increased and the size became larger, as compared with those in the corresponding ribbons due to the relatively slow cooling rates (Figs. 4d and 4f). However, almost no nanocrystals were seen in the as-cast, 3 mm rod of alloy Cu0.3 (Fig. 4e), confirming that the optimum Cu doping indeed enhance the GFA.

Additionally, the crystallization resistance of the aforementioned ribbons and rods samples has also been investigated in detail. The corresponding HRTEM images and SAED patterns of the Cu0, Cu0.3, and Cu0.7 specimens annealed at 729 K ($\sim$50 K below $T_g$) for 30 min, are shown in Fig. 5, respectively. The volume fraction of the precipitated nano-sized crystals at the same heat-treatment condition for the ribbons and rods was illustrated in Fig. 1a. For the annealed Cu0 ribbon, the pre-existed α-Fe nano-clusters grew to an average size of 4–5 nm and some new α-Fe crystals also formed, leading to $\sim$3% volume fraction of the crystals in total (Figs. 1a and 5a). Compared with those in the ribbons, the size of the α-Fe nanocrystals contained in the annealed Cu0 rods is larger (i. e., 5–7 nm) and the amount is increased to 4% volume fraction (Figs. 1a and 5d). However, for the heat-treated Cu0.3 alloy specimen, very few α-Fe nanocrystals precipitated in the amorphous matrix in both the ribbon and rod specimens (Figs. 5b and 5e). In the annealed Cu0.7 ribbons, the nanosized grains become even larger and their volume fraction is increased to more than 10% (Fig. 5c). Local FFT analysis of some large nanosized particles was performed and the patterns can be indexed as α-Fe (inset of Fig. 5c). Similarly, larger and more nanocrystals were precipitated in the annealed Cu0.7 rods (Fig. 5f). Thus, it can be confirmed that the optimum Cu doping level can suppress formation of the α-Fe crystals and increase the crystallization resistance. To confirm this hypothesis, the activation energy for crystallization which generally relates to the difficulty in atomic diffusion and rearrangement were estimated for all three
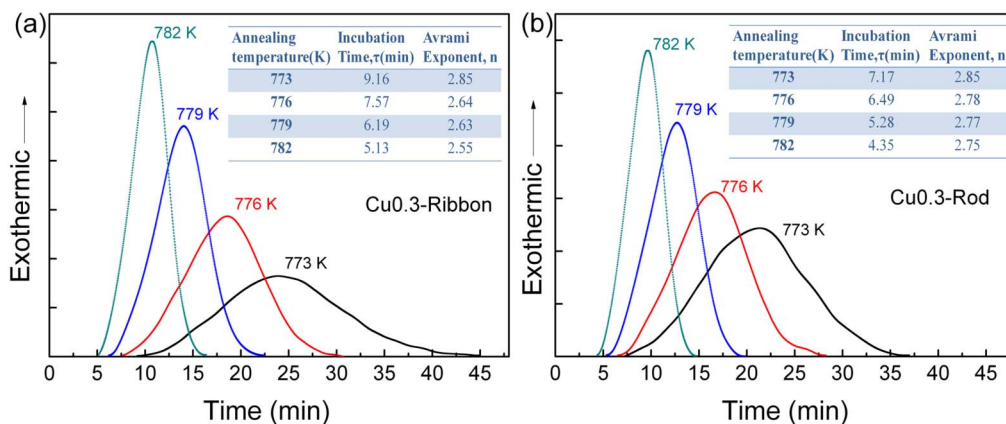


**Figure 3 | The isothermal DSC curves for the Cu0.3 ribbon (a) and rod (b) at different annealing temperatures of 773, 776, 779 and 782 K.**
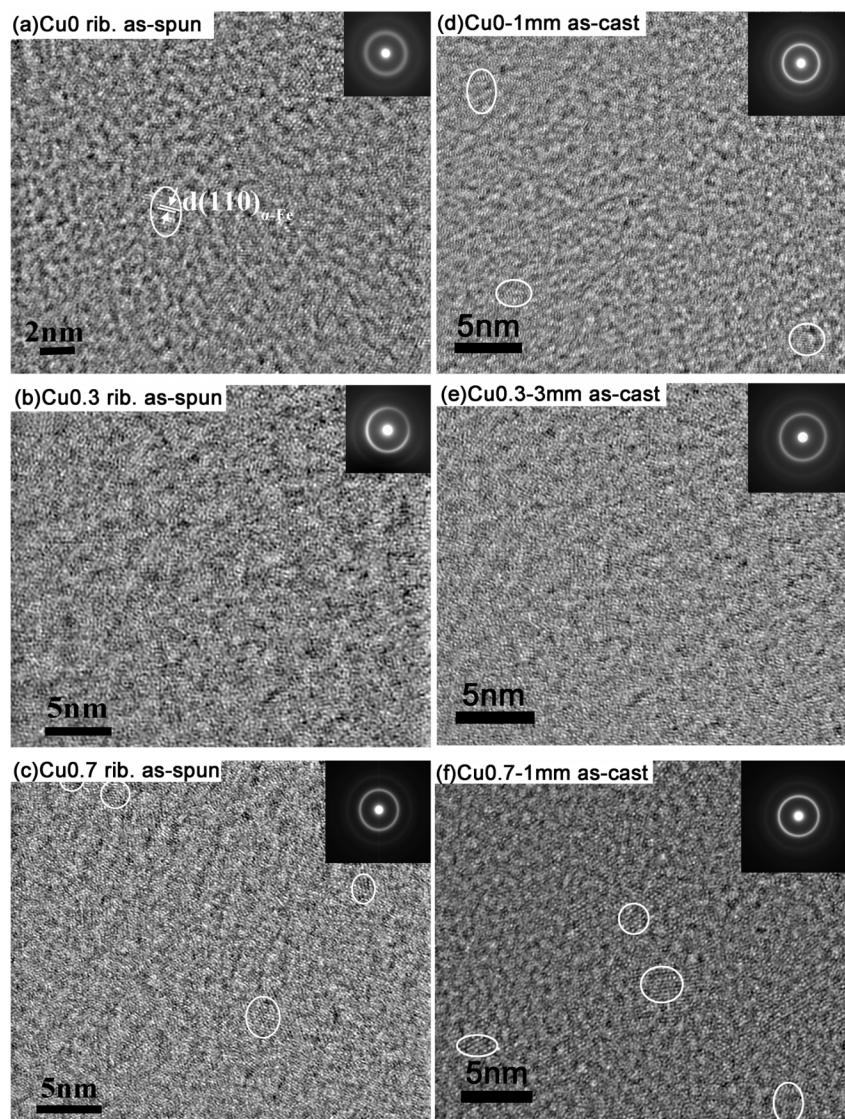
**Figure 4 | HRTEM images and SAED patterns of the as-cast ribbons and rods of the investigated alloys.** (a) Cu0, as-spun ribbon, (b) Cu0.3, as-spun ribbon, (c) Cu0.7, as-spun ribbon, (d) Cu0, as-cast rod, (e) Cu0.3, as-cast rod, (f) Cu0.7, as-cast rod.

alloys by DSC measurements at various heating rates. The activation energy for crystallization of the α-Fe phase can be determined by the Kissinger equation[41]:

$$ln\left(\frac{T^2}{\beta}\right) = \frac{E_a}{RT} + const. \tag{3}$$

where β, $E_a$, R and T are the heating rate, activation energy, gas constant and specific temperature, i.e. the temperature of the first crystallization peak value, respectively. The activation energy for crystallization can then be derived by plotting the curve of $ln\left(\frac{T^2}{\beta}\right)$ versus 1/RT which displays approximately a straight line with a slope equal to $E_a$ as shown in Fig. 2b and the corresponding activation energy data was also tabulated in Table 1. One can see, indeed, the Cu0.3 alloy has the maximum value of the activation energy among all the investigated alloys (i.e., 470.9 kJ/mol), further verifying its largest crystallization resistance.

In addition to the HRTEM studies, the pair distribution function (PDF) analysis was used to reveal the structure changes at various length scales for both as-cast and annealed specimens of the Cu0 and Cu0.3 glassy ribbons. The structure factor, S(Q), and the corresponding PDF curves for these samples are presented in Fig. 6. It is found

that the as-quenched Cu0 and Cu0.3 samples show a similar pattern with no indication of the pre-existed α-Fe clusters, suggesting that either their sizes or total fraction is too small to be detected. After being annealed at 729 K for 30 min, the Cu0 alloy exhibits obvious ordering at the medium-to-long range scale whereas the Cu0.3 alloy basically show the same S(Q)-Q pattern as that of the as-cast sample. Furthermore, one can see that the first peak sharpened and small crystalline peak developed on the shoulder in the low Q region (i.e., at the medium-range length scale) for the annealed sample of the alloy Cu0, while no additional peaks can be observed in the pattern of the annealed Cu0.3 specimen. Thus, the above analyses have validated that appreciable medium-to-long range ordering occurred in the Cu0 alloy upon annealing but not in the Cu0.3 alloy. In other words, the addition of 0.3% Cu into the alloy can effectively increase its structural stability and crystallization resistance.

To further understand roles of Cu in glass formation, the atom probe tomography (APT) analysis of the current as-cast and annealed glassy ribbons were conducted. A 10-nm-thick section of an atom map and a corresponding elemental concentration profile along the length direction of the annealed Cu0.3 ribbons are shown in Figs. 7a and 7b, respectively. A 10% Cu iso-concentration surface for the annealed Cu0.7 ribbon is shown in Fig. 7c. Based on the APT
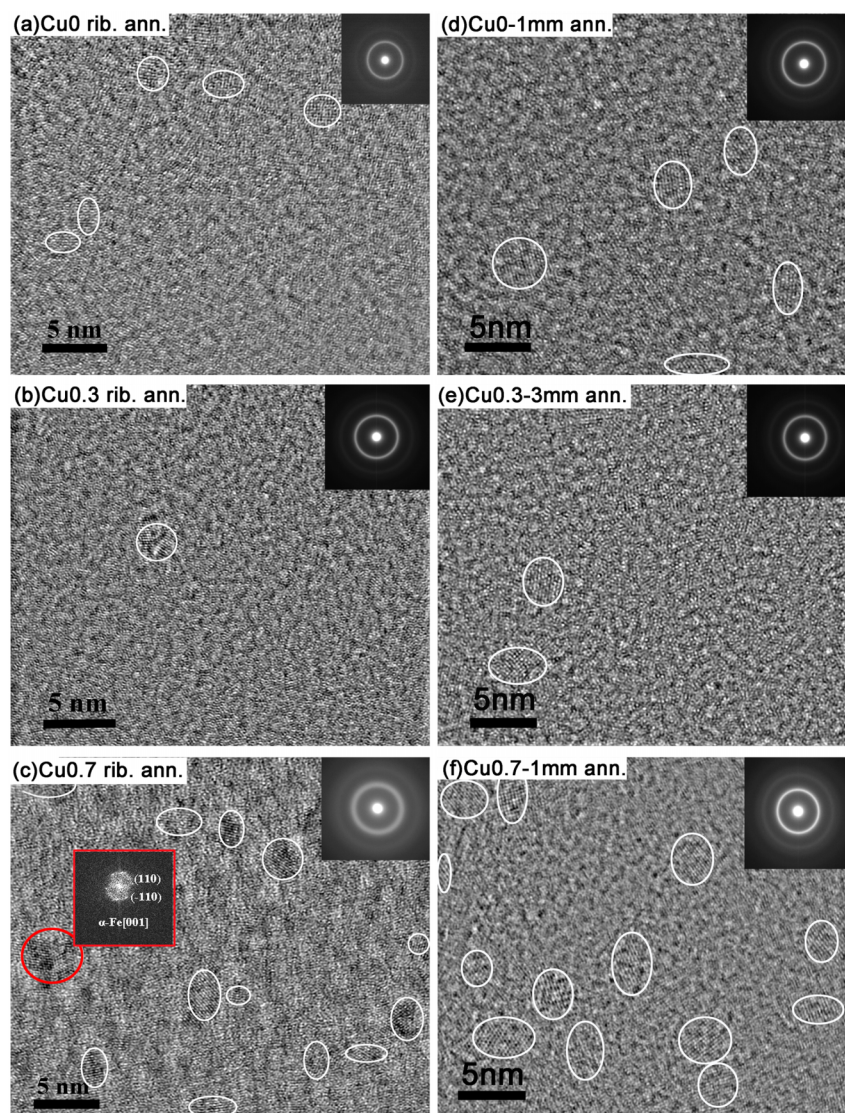
**Figure 5 | HRTEM images and SAED patterns of the annealed ribbons and rods of the investigated alloys.** (a) Cu0, annealed ribbon, (b) Cu0.3, annealed ribbon, (c) Cu0.7, annealed ribbon, (d) Cu0, annealed rod, (e) Cu0.3, annealed rod, (f) Cu0.7, annealed rod.

data, no evidence of phase separation was observed in both the as-cast and annealed specimens. For the annealed Cu0.3 alloy, only amorphous phase without any nanosized clusters was seen, which is consistent with the HRTEM and S(Q)-Q results shown in Figs. 5b and 6c,respectively. The compositional profile shown in Fig. 7b confirms that all the elements are homogeneously distributed with no sign of any chemical segregation. In the annealed Cu0.7 alloy, however, a large number of ultrafine spherical Cu-rich precipitates (less than 5 nm), as shown in Fig. 7c. More interestingly, many small regions (below 2 nm) where the atomic density of Fe and C, respectively, are concentrated were observed (as an example, the C distribution is shown in Fig. 7d). These locations are probably the precursors to devitrification, i.e., the crystallization embryos. Due to the limited size, the atomic packing of these tiny clusters could only be identified by the method proposed recently[42]. From the APT data, it is important to point out that some of the nanocrystals shown in Fig. 5c are spherical Cu-rich precipitates.

## Discussion
Glass formation in metallic liquids is essentially a competing process between liquid phases and the related crystalline phases[43,44]. Any factors which can increase liquid phase stability and crystallization

resistance would enhance the GFA. From Figs. 4, 5, 6 and 7, it is clear that doping 0.3% Cu in the alloy can effectively suppress formation of pre-existed $\alpha$-Fe clusters in the undercooled liquid. The APT data (Figs. 7a and 7b) have verified that the Cu element is solid-solutionized in the amorphous matrix (i.e., homogenously distributed). Upon undercooling, due to its high concentration, iron atoms tend to segregate to form clusters. With 0.3% Cu addition, redistribution of the Cu atoms is necessary, thus hindering the formation of $\alpha$-Fe (i.e., higher liquid phase stability) and resulting in higher GFA. Nevertheless, with an excessive addition of Cu (i.e. $\geq$0.7%), due to the intrinsic repulsive force between Fe and Cu atoms, copper atoms would agglomerate and form ultrafine spherical Cu precipitates, as demonstrated by the APT results in Fig. 7c and in a Cu-overdosed Fe-based alloy[45]. These Cu-rich clusters can act as nucleation sites of the $\alpha$-Fe clusters and make precipitation of $\alpha$-Fe even easier upon sub-sequent annealing. As such, the GFA in the overdosed alloys is dete-riorated. Similarly, during nanocrystallization of the Cu0.3 glass, which is a kind of diffusion-controlled three-dimensional growth as proved from the transformation kinetic analysis shown in Fig. 3, long-range diffusion of Cu atoms is needed to form the $\alpha$-Fe crystals due to the immiscibility between Cu and Fe. In other words, crystal-lization becomes difficult because of a higher activation energy

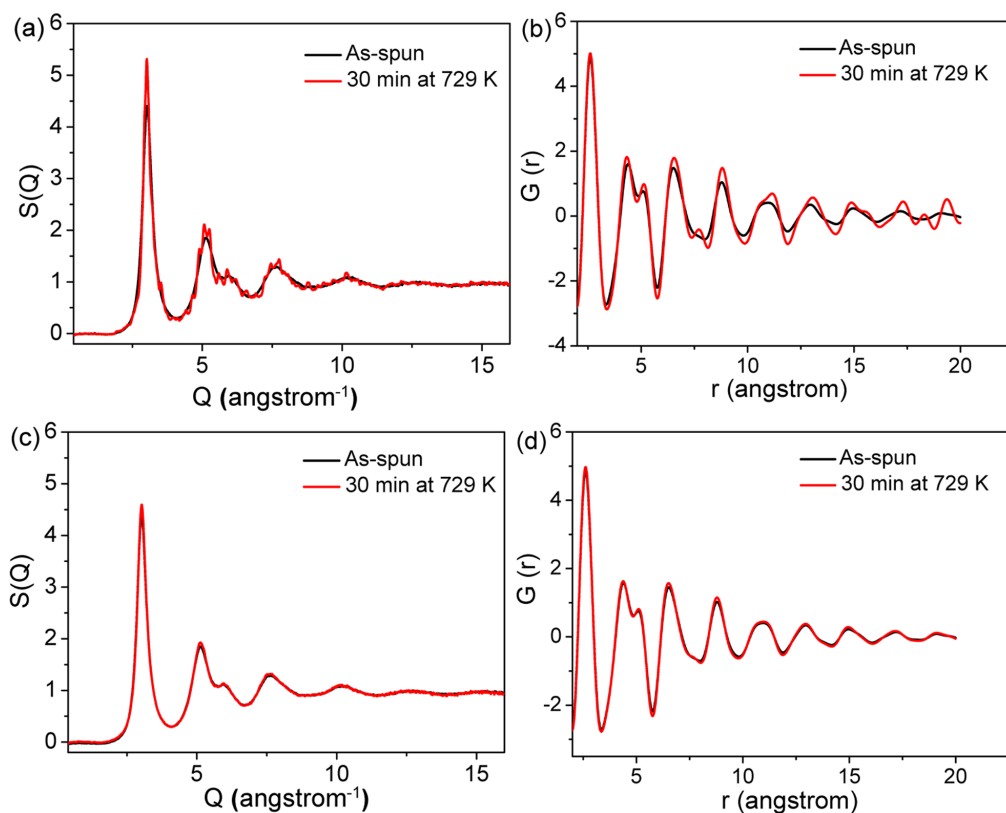**Figure 6 | The structure factor, S(Q), and the reduced pair-distribution function, G(r), for the as-cast and annealed specimens of the Cu0 and Cu0.3 alloys.** (a) Cu0, S(Q), (b) Cu0, G(r), (c) Cu0.3, S(Q), and (d) Cu0.3, G(r).
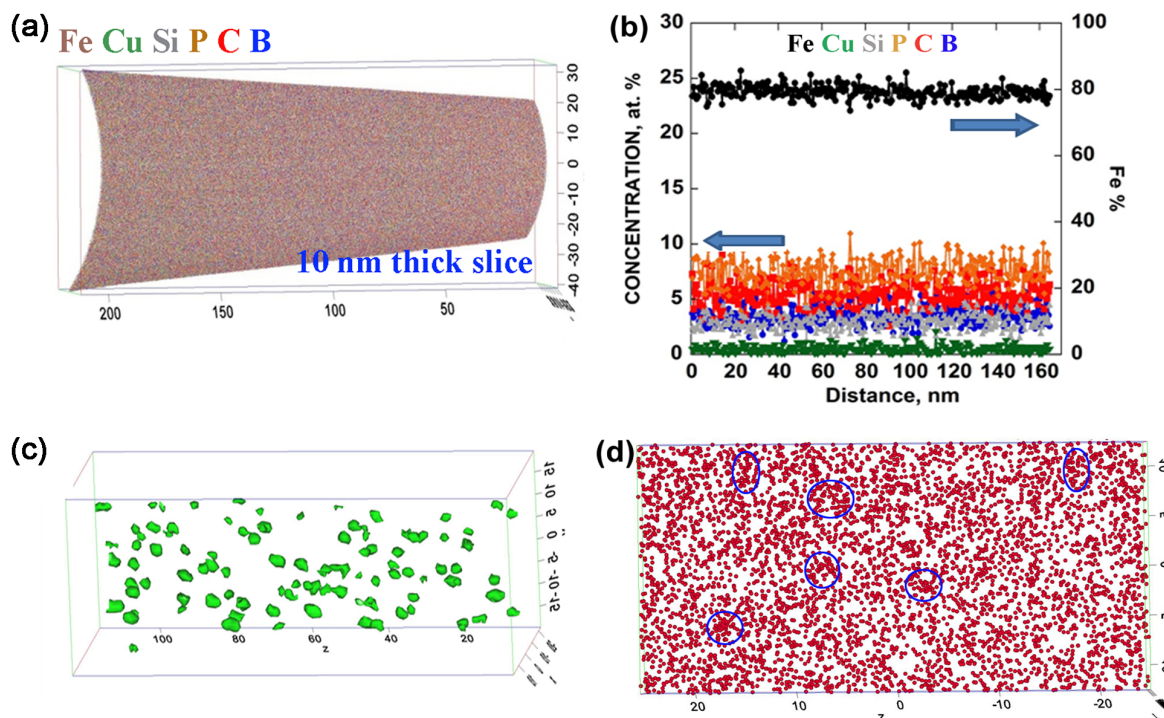


**Figure 7 | A 10 nm thick atom map of the annealed Cu0.3 alloy (a) and the corresponding elemental concentration profile (b) along the length direction.** The 10% Cu iso-concentration surface of the annealed Cu0.7 alloy and totally 102 Cu-rich precipitates were observed in this volume (c), and the corresponding atom map of the C distribution (d). The circles in (d) indicates the locations which the C atoms are concentrated.

barrier needed to overcome. Consequently, GFA in the Cu0.3 alloy is greatly enhanced due to an increase in crystallization resistance. Nevertheless, excessive Cu doping will inevitably stimulate formation of Cu-enriched regions which separates from the amorphous matrix. These small Cu-enriched sites could be nucleation sites of the α-Fe clusters, thereby accelerating the nucleation and lowering the activation energy for crystallization (e.g., 403.4 kJ/mol of alloy Cu0.7 shown in Table 1 and Fig. 2b). As a result, the GFA in these alloys was decreased because of the easier formation of the α-Fe crystals.

In summary, we manifested that an appropriate amount of Cu additions which has a positive enthalpy of mixing with Fe is remarkably effective in enhancing the GFA via stabilizing the glass-forming liquid and concurrently increasing the resistance for crystallization. However, due to the repulsive nature between the Fe and Cu atoms, an excessive Cu addition would cause Cu-clustering which, by providing nucleation sites, will stimulate copious crystallization of α-Fe, thus deteriorating the GFA[45,46]. Consequently, the optimum amount of Cu additions is dictated by the competition between the structural homogeneity of glassy-forming liquids and their tendency toward Cu-clustering. Different from the traditional strategy, our current findings, i.e. by doping the elements which has a positive mixing enthalpy with main constituents in the alloy, provide new insights for understanding glass formation in alloys with a high solvent content and also of great importance for developing novel Fe-based BMGs concurrently possessing high GFA and high saturation magnetization. Implementing the same method, we have successfully developed a new series of Al-rich $(Al_{0.86}La_{0.05}Ni_{0.09})_{1-x}Sn_x$ (x = 0.1% to 0.5% by an increment of 0.1%) glassy alloys with minor additions of Sn which has a positive enthalpy of mixing with Al (+4 kJ/mol[47]).The optimum doping amount turns out to be ~0.2% that results in an improvement in the GFA by ~30% in terms of the critical glass-forming thickness of the BMGs produced by wedge-casting, which will be reported elsewhere[48]. The strategy applied in other alloy systems such as Co-based, Ni-based BMGs for enhancing the GFA is being tested currently.

## Methods

**Preparation of samples.** Alloy ingots with nominal compositions of $Fe_{76-x}C_{7.0}Si_{3.3}B_{5.0}P_{8.7}Cu_x$ (x = 0, 0.3, 0.7, 1.0 at. %, hereafter designated as Cu0, Cu0.3, Cu0.7, Cu1.0, respectively) were prepared by arc-melting mixtures of pure elements (99.9 %) and the Fe-P alloys (P: 26.28, Si:0.01, C:0.02, Mn:0.69, Ti:0.35, Ca:0.01, S: 0.01 wt%) under an argon atmosphere followed by suction casting into cylindrical rods with 1 to 4 mm in diameter and 70 mm in length. Ribbon samples with a width of 1–2 mm and a thickness of 30–50 μm were prepared using the melt-spinning technique.

**Thermal analysis.** The annealing experiments were carried out in a vacuum furnace at 729 K for 30 min. Thermal properties associated with glass transition, supercooled liquid and crystallization event were examined by differential scanning calorimetry (DSC) in a Netzsch STA449C apparatus at a heating rate from 10 to 40 K/min. For the isothermal DSC measurements, the same apparatus was used and the annealing temperatures were chosen to be 773, 776, 779 and 782 K for the as-cast Cu0.3 rod and ribbon, respectively. The activation energy of the crystallization process was estimated by Kissinger analysis based on the first exothermal peak temperature of crystallization $T_{p1}$. The melting and solidification behavior were investigated by using differential thermal analysis (DTA) at a heating rate of 20 K/min.

**HRTEM, EPMA and APT analysis.** Structures of the as-cast and annealed ribbons and rods were characterized by high resolution transmission electron microscopy (HRTEM) and x-ray diffraction (XRD) with Cu $K_\alpha$ radiation. For the rod specimens, the central area was selected for the HRTEM analysis. The HRTEM specimens were prepared by an ion milling method and the HRTEM observation were carried out using a JEM-2100 microscope. Fast Fourier transformation (FFT) and inverse fast Fourier transformation (IFFT) were conducted to the HRTEM images and the noise was subtracted to make the images clearer. Local FFT analyses were also conducted to analyze the structure of the precipitated nano-clusters. Composition analyses of the as-cast and annealed samples were carried out using an electron probe micro-analyzer (EPMA, JEOL JXA-8100). Needle-shaped specimens for atom probe tomography (APT) were fabricated by a lift-out method in a FEI Nova™ 200 Nanolab™ focused ion beam instrument[49,50]. The APT analyses were performed in a Cameca Instruments LEAP 4000X HR in either voltage or laser (λ= 400 nm, 100 kHz pulse repetition rate) modes.

**Pair distribution function analyses.** High energy synchrotron x-ray diffraction measurements of the as-spun and annealed ribbons have been carried out to determine their pair distribution functions (PDFs), using beamline 11-ID-C at the Advanced Photon Source, Argonne National Laboratory (ANL). The energy of the incident monochromatic x-ray beam was 115 keV and a beam size of 150 μm × 150 μm was used. The diffracted x-rays were collected using a Perkin-Elmer area detector which was placed at 36 cm behind the specimen. The diffraction data, as a function of momentum transfer (Q, up to 25 Å$^{-1}$), were recorded at room temperature for 50 seconds for each sample, where $Q=4\pi \sin \theta/\lambda$, $\lambda$ (=0.10798 Å) is the x-ray wavelength and $2\theta$ is the diffraction angle. The structure factor $S(Q)$ was then determined by analyzing the diffraction data using the program PDFgetX2 with subtraction of background and corrections for polarization, fluorescence, absorption and inelastic scatting[51].The reduced PDF [$G(r)$, where $r$ is the atomic separation] was thus obtained by the Fourier transform of the $S(Q)$[52]

$$G(r)=\frac{2}{\pi}\int_0^\infty Q[S(Q)-1]\sin (Qr)dQ=4\pi r[\rho(r)-\rho_0] \qquad (4)$$

where $\rho_0$ is the sample number density, and $\rho(r)$ is the microscopic number density.

1. Makino, A. *et al*. The effect of Cu on the plasticity of Fe-Si-B-P-based bulk metallic glass. *Scripta Mater.* **60**, 277–280 (2009).
2. Makino, A. *et al*. Low core losses and magnetic properties of $Fe_{85-86}Si_{1-2}B_8P_4Cu_1$ nanocrystalline alloys with high B for power applications(invited). *J. Appl. Phys.* **109**, 07A302 (2011).
3. Urata, A., Yamaki, M., Takahashi, M., Okamoto, K. & Matsumoto, H. Low core loss of non-Si quaternary $Fe_{83.3}B_8P_8Cu_{0.7}$ nanocrystalline alloy with high $B_s$ of 1.7T. *J. Appl. Phys.* **111**, 07A335 (2012).
4. Chiba, M., Urata, A., Matsumoto, H., Yoshida, S. & Makino, A. Characteristics of Fe-Si-B-P-Cu nanocrystalline soft magnetic alloy powders with high $B_s$. *IEEE Trans. Magn.* **47**, 2845 (2011).
5. Wu, R. I., Wilde, G. & Perepezko, J. H. Glass formation and primary nanocrystallization in Al-base metallic glasses. *Mater. Sci. Eng. A* **301**, 12 (2001).
6. Perepezko, J. H., Hebert, R. J., Wu, R. I. & Wilde, G. Primary crystallization in amorphous Al-based alloys. *J. Non-crystal. Solids* **317**, 52–61 (2003).
7. Boucharat, N., Rosner, H., Perepezko, J. H. & Wilde, G. Devitrification of Al-based glass forming alloys. *Mater. Sci. Eng. A* **375–377**, 713–717 (2004).
8. Yoshizawa, Y., Oguma, S. & Yamauchi, K. New Fe-based soft magnetic alloys composed of ultrrafine grain structure. *J. Appl. Phys.* **64**, 6044–6046 (1998).
9. Yoshizawa, Y., Yamauchi, K., Yamane, T. & Sugihara, H. Common mode choke cores using the new Fe-based alloys composed of ultrafine grain structure. *J. Appl. Phys.* **64**, 6047–6049 (1988).
10. Makino, A. *et al*. Applications of Nanocrystalline Soft Magnetic Fe-M-B (M = Zr, Nb) Alloys, NANOPERM(R). *IEEE Trans. Magn.* **33**, 3793–3798 (1997).
11. Schwarz, R. B., Shen, T. D., Harms, U. & Lillo, T. Soft ferromagnetism in amorphous and nanocrystalline alloys. *J. Magn. Magn. Mater.* **283**, 223–230 (2004).
12. Li, H. X. *et al*. Glass formation and magnetic properties of the Fe-C-Si-B-P-(Cr-Al-Co) bulk metallic glasses fabricated using industrial raw materials. *J. Magn. Magn. Mater.* **321**, 283–2837 (2009).
13. Li, H. X., Jung, H. Y. & Yi, S. Glass forming ability and magnetic properties of bulk metallic glasses $Fe_{68.7-x}C_{7.0}Si_{3.3}B_{5.5}P_{8.7}Cr_{2.3}Mo_{2.5}Al_{2.0}Co_x$ (x = 0–10). *J. Magn. Magn. Mater.* **320**, 241–245 (2008).
14. Makino, A., Men, H., Kubota, T., Yubuta, K. & Inoue, A. FeSiBPCu nanocrystalline soft magnetic aAlloys with high $B_s$ of 1.9 tesla produced by crystallizing hetero-amorphous phase. *Mater. Trans.* **50**, 204–209 (2009).
15. Makino, A., Men, H., Kubota, T., Yubuta, K. & Inoue, A. New Fe-metalloids based nanocrystalline alloys with high $B_s$ of 1.9T and excellent magnetic softness. *J. Appl. Phys.* **105**, 07A308 (2009).
16. Makino, A., Men, H., Yubuta, K. & Kubota, T. Soft magnetic FeSiBPCu heteroamorphous alloys with high Fe content. *J. Appl. Phys.* **105**, 013922 (2009).
17. Makino, A., Men, H., Kubota, T., Yubuta, K. & Inoue, A. New Excellent Soft Magnetic FeSiBPCu Nanocrystallized Alloys With High $B_s$ of 1.9 T From Nanohetero-Amorphous Phase. *IEEE Trans. Magn.* **45**, 4302–4305 (2009).
18. Makino, A. Nanocrystalline soft magnetic Fe-Si-B-P-Cu alloys with high B of 1.8-1.9T contributable to energy saving. *IEEE Trans. Magn.* **48**, 1331 (2012).
19. Fan, X. *et al*. Fe-based nanocrystalline FeBCCu soft magnetic alloys with high magnetic flux density. *J. Appl. Phys.* **109**, 07A314 (2011).
20. Kong, F. *et al*. High $B_s$ $Fe_{84-x}Si_4B_8P_4Cu_x$ (x = 0–1.5) nanocrystalline alloys with excellent magnetic softness. *J. Appl. Phys.* **109**, 07A303 (2011).
21. Urata, A., Matsumoto, H., Sato, S. & Makino, A. High $B_s$ nanocrystalline alloys with high amorphous-forming ability. *J. Appl. Phys.* **105**, 07A324 (2009).
22. Stoica, M. *et al*. $[(Fe_{0.5}Co_{0.5})_{0.75}B_{0.20}Si_{0.05}]_{96}Nb_4$ metallic glasses with small Cu additions. *Metal. Mater. Trans. A* **42A**, 1476–1480 (2011).
23. Stoica, M. *et al*. FeCoBSiNb bulk metallic glasses with Cu additions. *Physica Status Solid C-Current Topics in Solid State Physics* **7**, 1331–1335 (2010).
24. Li, R., Stoica, M. & Eckert, J. Effect of minor Cu addition on phase evolution and magnetic properties of $\{[(Fe_{0.5}Co_{0.5})_{0.75}Si_{0.05}B_{0.20}]_{0.96}Nb_{0.04}\}_{100-x}Cu_x$ alloys. *J. Phys.: Conf. Ser.* **144**, 012042 (2009).

25. Chau, N., Luong, N. H., Chien, N. X., Thanh, P. Q. & Vu, L. V. Influence of P substitution for B on the structure and properties of nanocrystalline $Fe_{73.5}Si_{15.5}Nb_3Cu_1B_{7-x}P_x$ alloys. *Phys. B* **327**, 241–243 (2004).

26. Zeng, Y. Q., Inoue, A., Nishiyama, N. & Chen, M. W. Remarkable effect of minor boron doping on the formation of the largest size Ni-rich bulk metallic glasses. *Scripta Mater.* **60**, 925–928 (2009).

27. Wang, W. H., Dong, C. & Shek, C. H. Bulk metallic glasses. *Mater. Sci. Eng. R* **44**, 45–89 (2004).

28. Liu, C. T. & Lu, Z. P. Effect of minor alloying additions on glass formation in bulk metallic glasses. *Intermetallics* **13**, 415–418 (2005).

29. Lu, Z. P. & Liu, C. T. Role of minor alloying additions in formation of bulk metallic glasses: a review. *J. Mater. Sci.* **39**, 3965–3974 (2004).

30. Wang, W. H. Roles of minor additions in formation and properties of bulk metallic glasses. *Prog. Mater. Sci.* **52**, 540–596 (2007).

31. Zhang, B., Wang, R. J., Zhao, D. Q., Pan, M. X. & Wang, W. H. Superior glass-forming ability through microalloying in cerium-based alloys. *Phy. Rev. B* **73**, 092201 (2006).

32. Xi, X. K., Li, L. L., Zhang, B., Wang, W. H. & Wu, Y. Correlation of atomic cluster symmetry and glass-forming ability of metallic glasses. *Phys. Rev. Lett.* **99**, 095501 (2007).

33. Inoue, A. Stabilization of metallic supercooled liquid and bulk amorphous alloys. *Acta Mater.* **48**, 279–306 (2000).

34. Greer, A. L. Confusion by design. *Nature* **366**, 303–304 (1993).

35. Senkov, O. N. & Miracle, D. B. Effect of the atomic size distribution on glass forming ability of amorphous metallic alloys. *Mater. Res. Bull.* **36**, 2183–2198 (2001).

36. Takeuchi, A. & Inoue, A. Classification of bulk metallic glasses by atomic size difference, heat of mixing and period of constituent elements and its application to characterization of the main alloying element. *Mater. Trans.* **46**, 2817–2829 (2005).

37. Chen, L. C. & Spaepen, F. Calorimetric evidence for the micro-quasicrystalline structure of 'amorphous' Al/transition metal alloys. *Nature* **336**, 366–368 (1988).

38. Yang, L. *et al.* Consecutive nucleation event during divetrification of $Zr_{52.5}Cu_{17.9}Ni_{14.6}Al_{10}Ti_5$ bulk metallic glass. *Adv. Eng. Mater.* **10**, 1043–1047 (2008).

39. Hu, L. & Ye, F. Crystallization kinetics of $Ca_{65}Mg_{15}Zn_{20}$ bulk metallic glass. *J. alloys Compd.* **557**, 160–165 (2013).

40. Christian, J. W. The Theory of Transformations in Metals and Alloys, 3rd ed., Pergamon, Oxford, (2002).

41. Kissinger, H. E. Reaction kinetics in differential thermal analysis. *Anal. Chem.* **29**, 1702–1706 (1957).

42. Hirata, A. *et al.* Direct observation of local atomic order in a metallic glass. *Nat. Mater.* **10**, 28–33 (2011).

43. Lu, Z. P., Liu, C. T., Thompson, J. R. & Porter, W. D. Structural amorphous steels. *Phys. Rev. Lett.* **92**, 245503 (2004).

44. Li, H. X., Gao, J. E., Jiao, Z. B., Wu, Y. & Lu, Z. P. Glass-forming ability enhanced by proper additions of oxygen in a Fe-based bulk metallic glass. *Appl. Phys. Lett.* **95**, 161905 (2009).

45. Hono, K., Ping, D. H., Ohnuma, M. & Onodera, H. Cu clustering and Si partitioning in the early crystallization stage of a $Fe_{73.5}Si_{13.5}B_9Nb_3Cu_1$ amorphous alloy. *Acta Mater.* **47**, 997–1006 (1999).

46. Ayers, J. D., Harris, V. G., Sprague, J. A., Elam, W. T. & Jones, H. N. On the formation of nanocrystals in the soft magnetic alloy $Fe_{73.5}Nb_3Cu_1Si_{13.5}B_9$. *Acta Mater.* **46**, 1861–1874 (1998).

47. de Boer, F. R., Boom, R., Mattens, W. C. M., Miedema, A. R. & Niessen, A. K. Cohesion in Metals: Transition Metal Alloys [de Boer, F. R., PettiFor, D. G. (ed.)] [45–52] (North-Holland, Amsterdam, 1988).

48. Chen, Z. P. *et al.* Alloying effects of the elements with a positive heat of mixing on the glass forming ability of Al-La-Ni amorphous alloys. *J. Alloys Compd.* submitted (2012).

49. Miller, M. K. Atom Probe Tomography, Kluwer Academic/Plenum Press, New York (2000).

50. Miller, M. K., Russell, K. F., Thompson, K., Alvis, R. & Larson, D. J. Review of atom probe FIB-based specimen preparation methods. *Microscopy and Microanalysis.* **13**, 428–436 (2007).

51. Qiu, X., Thompson, J. W. & Billinge, S. J. L. PDFgetX2: A GUI driven program to obtain the pair distribution function from X-ray powder diffraction data. *J. Appl. Cryst.* **37**, 678–678 (2004).

52. Egami, T. & Billinge, S. J. L. Underneath the bragg peaks: structural analysis of complex materials, Pergamon Press, Oxford (2003).

## Acknowledgements

## Author contributions

H.X.L., J.E.G., Y.W., Z.B.J. conceived and designed the experiments. Z.P.L. proposed the experiments ideas and analyzed the data. D.M., X.L.W., A.D.S. and Y.R. carried out the experiments about pair distribution functions. M.K.M. carried out the APT experiments. All the authors discussed the results and reviewed the manuscript.

## Additional information

**Supplementary information** accompanies this paper at http://www.nature.com/scientificreports

**Competing financial interests:** The authors declare no competing financial interests.

**How to cite this article:** Li, H.X. *et al.* Enhancing glass-forming ability via frustration of nano-clustering in alloys with a high solvent content. *Sci. Rep.* **3**, 1983; DOI:10.1038/srep01983 (2013).